Desalination and Water Treatment
www.deswater.com

doi:10.5004/dwt.2023.29146

281 (2023) 38–57
January

Comparative analysis of multi-effect distillation coupled with solar energy and combined cycle power plant

Muhammad Shoaib Malik, Ali Turab Jafry, Muhammad Asif*

Faculty of Mechanical Engineering, Ghulam Ishaq Khan Institute of Engineering Sciences and Technology, Topi 23460, Pakistan, Tel.: +92-938-281026; emails: masif@giki.edu.pk (M. Asif), toshoaibmalik@gmail.com (M.S. Malik), ali.turab@giki.edu.pk (A.T. Jafry)

Received 14 January 2022; Accepted 24 November 2022

ABSTRACT

To achieve a sustainable solution for water production and energy consumption, the present research performs a comparative analysis of multi-effect distillation (MED) coupled with solar energy and combined-cycle power plant (CCP). A numerical model of solar system is solved in Mathcad, and the validated model of MED and CCP are integrated using ASPEN PLUS® V8.8 as the process simulation tool. The impact of process parameters like number of MED effects, top brine temperature, feed salinity and heat input on gain output ratio (GOR) is investigated. The effect of change in feed salinity on total heat transfer area and steam consumption is explored. It is observed that increasing number of stages resulted in more distillate production. However, more number of stages led to higher capital cost as well as high distillate cost. In addition, an increase in feed salinity promoted the total heat transfer area and increased steam consumption which resulted in reduction of GOR. Economic comparison of both combinations of MED-CCP and MED-solar was carried out and return on investment was investigated. Economic analysis revealed that capital cost, operation cost and production cost was increased with increase in MED capacity. These costs were higher using solar energy as compared to CCP because the cost of steam obtained from the solar collectors was higher than the cost of steam generated by CCP. Return on investment for the MED-CCP combination was predicted as approximately six years for fixed MED capacity of 7000 m³/d.

Keywords: Desalination; Distillation; Multi-effect distillation; ASPEN PLUS simulation

1. Introduction

Although our earth's surface has abundance of water, however, only 0.3% is drinkable directly, the remaining 99.7% is spread in the form of brackish water, seawater, oceans, and icecaps [1,2]. Seawater is primarily made up of 96.5% water, 2.5% salts, and trace amounts of other substances such as dissolved inorganic and organic materials [3]. The shortage of fresh water is growing with the passage of time due to the steady increase in population. By 2025, it is possible that half of the world's population would reside in regions with limited water supplies. By 2030, there may be 700 million fewer people on the planet due to severe water scarcity. One in four children globally will be residing in locations with extremely high water stress by the year 2040 [4]. According to the 2018 edition of the United Nations World Water Development Report, nearly 6 billion people will experience clean water scarcity by 2050 [5]. Desalination of seawater is one option for dealing with this lack of potable water.

Norbert Rillieux, an African–American inventor, was the first to introduce the idea of an evaporator body in 1845 [6]. Despite the fact that evaporator development began in 1845, it appears that the first paper on modelling of the multi-effect distillation (MED) mechanism did not appear until 1928. Multi-stage evaporation is used not only in chemical industry where required solvent can be concentrated

* Corresponding author.

but can also be used for water desalination. In the chemical industry, the evaporated liquid is usually not the product, unless the solvent is recovered from a reaction. The process of evaporation consumes a lot of energy. The need to save energy spurred the creation of this multi-stage process, which requires additional equipment (investment) to reduce the overall quantity and cost of energy consumed. For more than a century, the procedure has been used for solution concentration, crystallization, and purification, and involves 2–4 stages, which are commonly referred to as effects. MED process with 2–16 stages is being used in desalination industry since 1950. Other evaporation methods, such as the multi-stage flash method, are less energy efficient than MED [7]. In most situations, the process is powered by a low-temperature energy source. In most industrial scenarios, this energy source is the waste steam from a steam-operated power plant, a source of heat in refineries, or other low-level steam or hot fluid from other sources [8]. Schematic diagram of MED process is shown in Fig. 1.

MED is a low-temperature thermal process for extracting fresh water by collecting vapor from boiling seawater in a succession of vessels (called effects), each of which is kept at a lower temperature than the one before it. The vapors produced in one effect can be used to heat the next, with the exception of the first (at maximum pressure), which needs an external heat source. This source of heat can be provided by the waste heat of combined cycle power plant or by solar renewable energy. Steam provided in the first effect will be produced from heating water through the waste heat from combined-cycle power plant (CCP) or solar energy which is then compressed to a certain pressure. In the first effect, the feed water is heated by this steam which passes in the tubes. Seawater is either uniformly distributed or sprayed on the tubes filled with hot steam and as a result, water evaporates leaving behind the salt rich water known as brine. The evaporated water (steam), then flows into the next effect (stage) where it heats and evaporates more seawater by condensing itself to become the product (fresh water).

Each effect basically recycles the energy from the earlier, however, the temperature and pressure keeps dropping subsequently. The steam from last effect is used to preheat the incoming seawater and considerably lowers the energy consumption in MED process. A vacuum pump/compressor is employed after the final condensation point to maintain the progressive pressure gradient within the vessel by eliminating the collected non-condensable gases as well as the leftover water vapor.

The pressure gradient along the MED effects is determined by the saturation pressure of the input stream and the condensing steam exiting the final level, which is condensed by chilling with saltwater. The typical pressure difference of 5–50 kPa are common throughout the system (less than 5 kPa/stage) [9]. The performance of an MED plant is judged by a very important parameter known as gain output ratio (GOR) which is the ratio of mass flow rate of the distillate to the mass flow rate of the heating steam in a thermal desalination process [10,11].

In recent years, there has been an increase in interest in the literature about the deployment of new multipurpose power plants as well as the retrofitting of existing single-purpose ones to produce power and water. By recovering and recycling the system's waste heat, existing single-purpose power plants can be transformed into multipurpose ones. In industrial desalination plants, waste heat can be converted to steam to produce fresh water while also being used for local heating and cooling. It is a difficult effort to build integrated power plants with desalination systems, because it frequently necessitates simultaneous optimization of several thermodynamic, financial, and environmental factors.

Since the MED technology can function at low temperatures (such as 70°C), it has the potential to be powered by solar energy. For high-temperature operation, MED might therefore be combined with flat plate solar collectors (FPCs), evacuated tube collectors (ETCs), parabolic trough collectors (PTCs), or even linear Fresnel collectors (LFCs). Additionally, photovoltaic panels that provide the necessary electric power to run the water pumps and vacuum might be added into the system. As a result, a MED process can be driven utilizing a variety of coupling approaches.

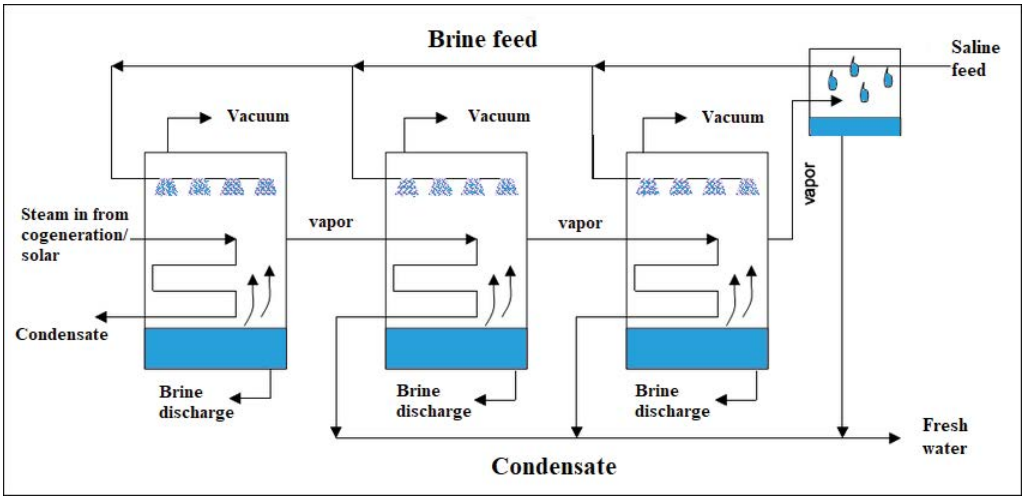

Fig. 1. MED schematic diagram.

The FPC, ETC, PTC, or LFC array in the earlier integration can generate sufficient heat to create the requisite motive steam to begin the MED operation.

Many researchers have presented their work on MED process including its modeling, simulation and thermal analysis. They have presented the idea of linking MED with different energy sources such as low-grade energy, solar energy and combined cycle power plant. Fiorini and Sciubba [12] used a modular simulator, CAMEL, to create a model for thermodynamic and thermo-economic simulation of an MED desalination plant. Belghaieb et al. [13] simulated and optimized a triple effect desalination MED unit. They studied the thermo-compression of vapors and the recycling of fraction of produced vapors. Roca et al. [14] presented dynamic simulation of a multi-effect distillation process under a variety of operating conditions. It was created with the goal of improving the process operation and developing a control strategy that maximizes distillate output. Ma et al. [15] developed three simulation models for the LT-MED (low-temperature multi-effect distillation) seawater desalination process up to four effects. The results showed that for TVC ejection, the process type, effect number and number of effects have a major impact on the efficiency, while the impact of heating steam temperature on performance was considerably less.

It is inferred from the literature that integration of MED with solar plant is one of the most promising technique. Sharaf et al. [16] thermo-economically evaluated various configurations of MED coupled with solar fields through solar collectors. Likewise, Ali et al. [17] presented a comprehensive techno-economic review of solar energy-based desalination processes and recommended solar-MED for large-scale solar desalination plants because of low water production cost. In another study, Ghenai et al. [18] performed parametric study and performance analysis of the hybrid MED adsorption desalination system powered by solar energy. In another study, Shahzad et al. [19] analyzed the hybrid integrated MED-adsorption cycle and figured out that the proposed method enhanced the water productivity and decreased the effect of fouling and scaling at latter stages.

Cogeneration can simultaneously meet energy and water demands. Almutairi et al. [20] presented an intriguing energy and exergetic analysis of a VC-MED (vapor-Compression MED) with a combined cycle providing steam for the ejector. A unique cogeneration system for power generation and seawater desalination was proposed by Luo et al. [21]. It combines a CRGT (chemically recuperated gas turbine) with a multi-effect thermal vapor compression desalination (MED-TVC) technology. The CRGT-MED dual-purpose system offers a lower product cost, higher thermal efficiency and a shorter payback time, making it a practical and appealing solution for water and power cogeneration. Recently, Chen et al. [22] presented techno-economic analysis of integrated vacuum MED and solar photovoltaic/thermal energy system for cogeneration of electricity and water. They predicted second law efficiency of 25% for photovoltaic module and 45% for thermal collectors with cost of water production in the range of 0.7–4.3 USD/m^3.

By exploring the previously reported prominent literature on MED, most research is carried out on thermodynamic analysis of MED when coupled with ORC, solar energy and other waste heat recovery processes. Most researchers have presented an idea of using renewable energy resources and waste heat for multi-effect distillation. The parametric study of MED model having seven effects/stages in parallel feed configuration is never discussed in any literature. A comparative analysis of cogeneration power plant and solar energy integrated with MED has never been presented in the literature. Economic analysis of MED-CCP and MED-solar is presented and then compared with each other which is one of the main novelties of this paper. In this work, we aim to present the comparison of an integration of multi-effect distillation with cogeneration power plant (MED-CCP) and solar energy (MED-solar). The main motivation of this comparison is to reduce the energy consumption and unit water cost and to find out the combination which is more economically and technically feasible.

Therefore, in this study, MED system was integrated with either CCP or solar collectors and the effect of process parameters like number of MED effects, top brine temperature (TBT), feed salinity and heat input on gain output ratio was analyzed to enhance the permeate flux and to improve the MED performance. The effect of change in feed salinity on total heat transfer area and steam consumption was explored. The impact of three different pressure steam (produced in CCP) on the production of permeate flux in MED system and loss in power output in CCP was investigated by changing their flow rates. Comparison of coupling MED with CCP and solar energy was carried out at constant permeate flux. The exergy analysis of two integrated system of MED-CCP and MED-solar was carried out in the form of exergy destruction at various operating conditions. Lastly, the economic comparison of both combinations of MED-CCP and MED-solar was carried out and return on investment (ROI) was predicted for the integrated system.

2. Process model

2.1. Energy analysis

The first law of thermodynamics was used to evaluate and examine the performance of energy systems. This principle is based on the energy conservation principle, which states that sum of all energies in a system remains constant. Under steady-state conditions, the general energy balance equation is as follows:

2.2. Mass balance

In the evaporator, mass balance can be expressed as:

$$\dot{m}_F = \dot{m}_V + \dot{m}_P \tag{1}$$

where $\dot{m}_F$, $\dot{m}_V$ and $\dot{m}_P$ are the mass flow rate (kg/s) of feed, vapor and product, respectively.

Salt balance in evaporator of MED is given by Eq. (2):

$$X_f \dot{m}_F = X_b \dot{m}_b \tag{2}$$

where X_f and X_b are the salt fraction in feed and brine respectively and $\dot{m}_b$ is mass flow rate of brine in kg/s.

2.3. Enthalpy balance

Enthalpy balance in evaporator is given by Eq. (3):

$$\dot{m}_F H_F + \dot{m}_S H_{VS} = \dot{m}_V H_{V1} + \dot{m}_P H_{P1} + \dot{m}_S H_{CS} \quad (3)$$

where $\dot{m}_S$ = mass flow rate of steam, kg/s; H_F: enthalpy of feed, kJ/kg; H_{VS}: enthalpy of saturated steam at temperature T_s, kJ/kg; H_{V1}: enthalpy of saturated steam at temperature T_1, kJ/kg; H_{P1}: enthalpy of concentrated vapor, kJ/kg; H_{CS}: enthalpy of condensate, kJ/kg.

2.4. Exergy analysis

At a suitable reference state, an energetic study of the MED desalination plant was carried out. Exergy evaluation is a critical tool for determining the performance of an energy system and identifying the locations and sources of energy degradation. The less efficient portions of the proposed system can be identified to determine the possibility for improvement. The maximum useful work that may be taken from a system under reversible conditions is known as exergy. As seen in Eq. (4), the total exergy of a stream can be separated into four parts:

$$\dot{E}_x = \dot{E}_{ke} + \dot{E}_{pe} + \dot{E}_{ph} + \dot{E}_{ch} \left(\text{kW}\right) \quad (4)$$

where $\dot{E}_{ke}$, $\dot{E}_{pe}$, $\dot{E}_{ph}$ and $\dot{E}_{ch}$ are the kinetic, potential, physical and chemical exergies respectively. Because of their minor impact in comparison to the physical and chemical exergies, the kinetic and potential exergies are thought to be inconsequential.

The physical and chemical exergy can be expressed by Eqs. (5) and (6):

$$\dot{E}_{ph} = \dot{m}\left[\left(h_s - h_o\right) - T_o\left(s_s - s_o\right)\right]\left(\text{kW}\right) \quad (5)$$

$$\dot{E}_{ch,w} = \dot{m}\sum w_k\left(\mu_k^s - \mu_k^o\right) \ \left(\text{kW}\right) \quad (6)$$

In Eqs. (5) and (6), subscript '*s*' denotes the initial state and '*o*' denotes the corresponding environmental or reference state. The chemical potential and mass fraction are denoted by μ and *w*, respectively. Sharqawy et al. [23,24] proposed validated correlations to assess the thermo-physical parameters of seawater streams. These equations give the specific enthalpy (*h*), and specific entropy (*S*) for both pure and saline water, respectively [25]:

$$h_w = 141.355 + 4202.070T - 0.535T^2 + 0.004T^3 \quad (7)$$

$$h_{sw} = h_w - w_s\begin{pmatrix} b_1 + b_2 w_s + b_3 w_s^2 + b_4 w_s^3 + b_5 T + b_6 T^2 \\ + b_7 T^3 + b_8 w_s T + b_9 w_s^2 T + b_{10} w_s T^2 \end{pmatrix} \quad (8)$$

$$S_w = 0.1543 + 15.383T - 2.996\times10^{-2} \times +8.193\times10^{-5}\times T^3 - 1.370\times10^{-7}\times T^4 \quad (9)$$

$$S_{sw} = S_w - w_s\begin{pmatrix} c_1 + c_2 w_s + c_3 w_s^2 + c_4 w_s^2 + c_5 T + c_6 T^2 \\ + c_7 T^3 + c_8 w_s T + c_9 w_s^2 T + c_{10} w_s T^2 \end{pmatrix} \quad (10)$$

In Eqs. (7)–(10), the temperature unit (*T*) is °C and the units for the specific entropy and specific enthalpy are J/kg·K and J/kg, respectively. Constants used for the calculation of thermodynamic properties are listed in Table 1.

Exergy destruction $\dot{E}_d$ is equal to exergy inlet $\dot{E}_{xl}$ minus exergy outlet $\dot{E}_{xe}$ and exergy loss $\dot{E}_l$ of system components. In the steady state analysis, these quantities are expressed as:

$$\dot{E}_d = \dot{E}_{xe} + \dot{E}_l - \dot{E}_{xl} \ \left(\text{kW}\right) \quad (11)$$

Because of irreversibilities in the system, exergy destruction is linked to entropy generation. Energy lost to the environment during or at the end of a process, such as brine in a desalination plant, is linked to exergy loss.

2.5. Cogeneration process

The integrated model of MED process coupled with cogeneration is developed using a commercial simulation tool known as ASPEN PLUS® V8.8.

This model is based on some assumptions such as:

- Model operates in steady state conditions.
- Temperature and pressure of the dead state are 25°C and 1 bar, respectively.
- Compressors, pumps, valves, and turbines are modelled adiabatically.
- Kinetic and potential energy changes are considered negligible in the system.
- Heat transfer and pressure drops are ignored in the pipe lines.

Table 1
Constants for the calculation of thermodynamic properties

b_1–b_5	b_6–b_{10}	c_1–c_5	c_6–c_{10}
$b_1 = -2.348\times10^4$	$b_6 = -4.417\times10^1$	$c_1 = -4.231\times10^2$	$c_6 = -1.443\times10^{-1}$
$b_2 = 3.152\times10^5$	$b_7 = 2.139\times10^{-1}$	$c_2 = 1.463\times10^4$	$c_7 = 5.879\times10^{-4}$
$b_3 = 2.803\times10^6$	$b_8 = -1.991\times10^4$	$c_3 = -9.880\times10^4$	$c_8 = -6.111\times10^1$
$b_4 = -1.446\times10^7$	$b_9 = 2.778\times10^4$	$c_4 = 3.095\times10^5$	$c_9 = 8.041\times10^1$
$b_5 = 7.826\times10^3$	$b_{10} = 9.728\times10^1$	$c_5 = 2.562\times10^1$	$c_{10} = 3.035\times10^{-1}$

2.5.1. Process description

An outline of the cogeneration process which includes gas turbine and steam generation sections is shown in Fig. 2.

The feedstock of this cogeneration process is natural gas, which contains methane (83.62 wt.%), ethane (7.33 wt.%), propane (7.25 wt.%) and argon (1.8 wt.%). Firstly, natural gas is mixed with compressed air as shown in Fig. 3. The gas is totally burnt in the burner, resulting in hot gas with a temperature of 979°C. To generate electricity, the hot gas has to run through a gas turbine. As a result, its temperature and pressure both decline. Isentropic efficiency and mechanical efficiency of gas turbine is assumed to be 80% respectively. In a nutshell, a gas turbine is a device that consumes natural gas to create electricity. Hot gases from outlet of gas turbine are introduced into heat recovery steam generator (HRSG) as shown in Fig. 4, and respective annotations are presented in Table 2. Three steam products, each at different pressure grades are obtained which are passed through intermediate pressure turbine (IP), low-pressure turbine (LP) and high-pressure turbine (HP) depending on their steam pressures. As a result of this, electrical power is produced. In short, steam generator recovers heat from the hot gas to generate electrical power and steam by using steam turbines.

2.5.2. Physical properties

The PR-BM property method (Peng–Robinson equation of state with Boston Mathias Modifications) was used for the properties of the natural gas and combustion products. For the steam system in the steam generation area, the STEAMNBS property method (applicable for pure water and steam with temperature ranges from 273 to 2,000 K and maximum pressure of 10,000 bar) was used.

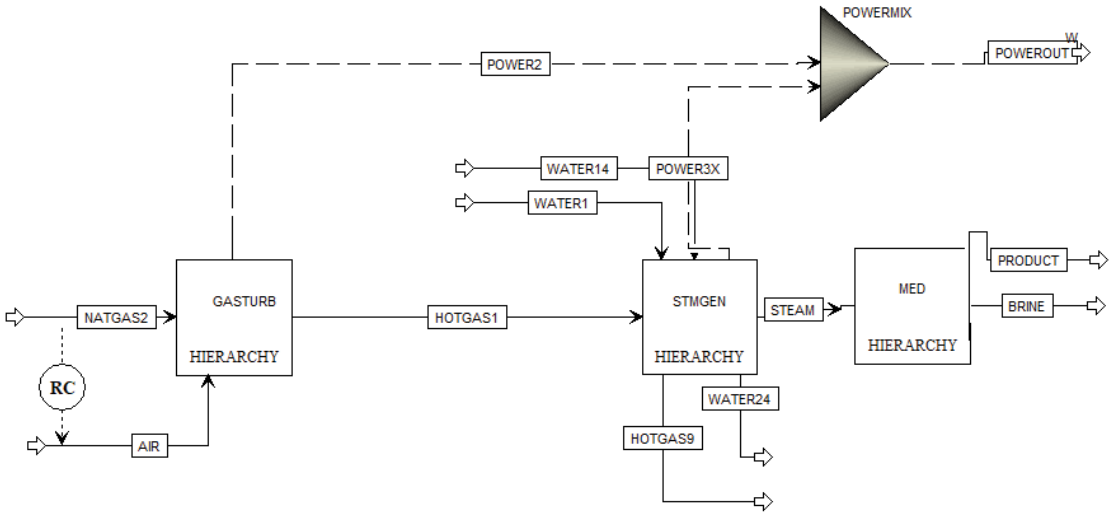

Fig. 2. Modelling and simulation of MED coupled with CCP in ASPEN PLUS® V8.8.

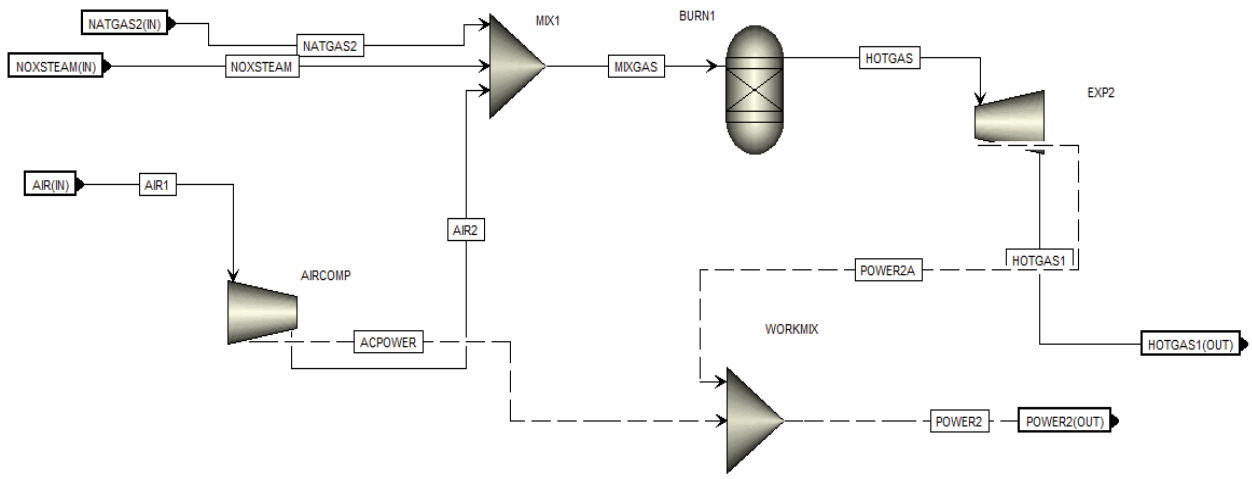

Fig. 3. Gas turbine model.

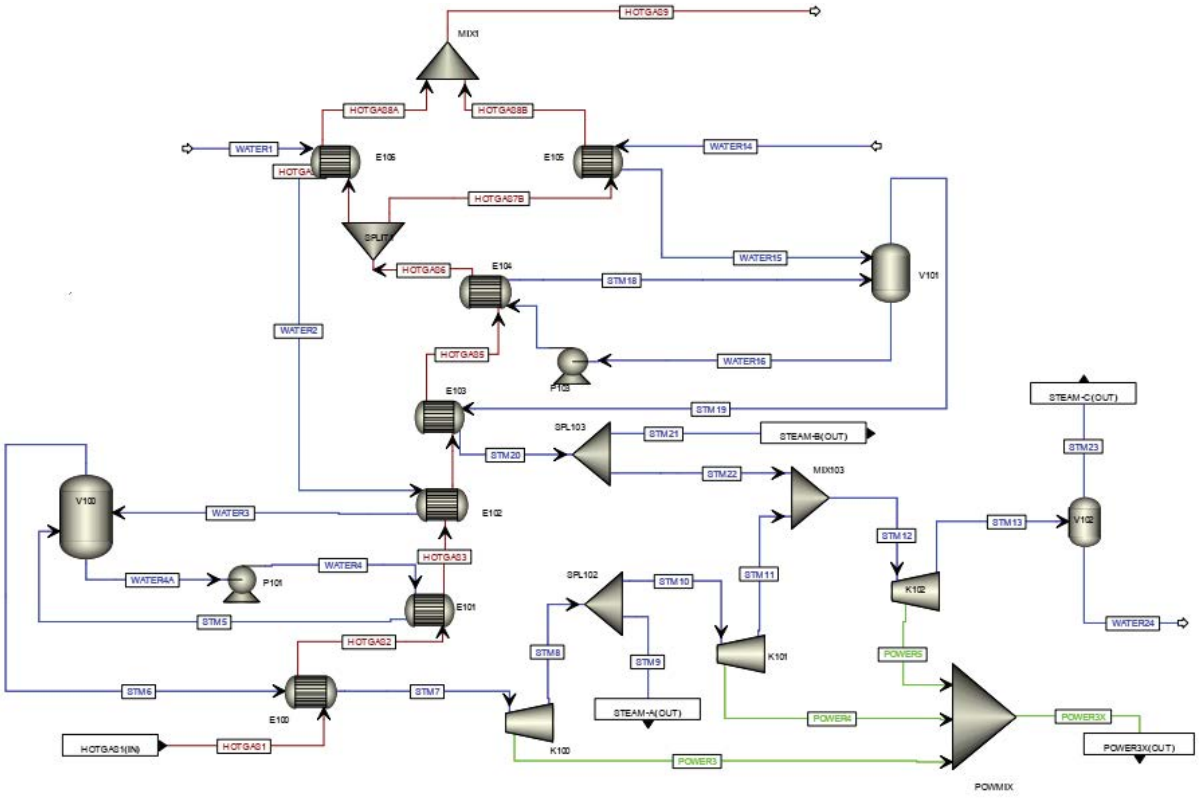

Fig. 4. Steam generator modelling.

Table 2
Full form of notations used in process models

Notations in process models	Full form
NATGAS2	Natural gas
NOXSTEAM	Steam
MIX1	Mixture
BURN1	Combustor
AIRCOMP	Compressor
GASTURB	Gas turbine
STMGEN	Steam generation
PRODUCT	Fresh water
BRINE	Salt rich water
POWEROUT	Total power output
MED	Multi-effect distillation plant

2.5.3. Chemical reactions

The only reactor unit in this process was the burner modelled with R Gibbs which uses the Gibbs free energy minimization method. This established the equilibrium composition of the products produced by the many reactions that might occur.

2.6. Solar energy process

A solar collector is a device which gathers energy from the sun by absorbing solar radiation. The coating and material type of solar collector is such that it maximizes solar energy absorption. Solar collector is mainly of two types: non-concentrating collectors and concentrating collectors. Flat plate collector (FPC) and evacuated tube collector (ETC) are non-concentrating collectors while concentrating collectors include compound parabolic collector (CPC), parabolic dish, parabolic trough, and solar tower. Some of the assumptions considered for solar collector field are:

- The entire system is in a quasi-equilibrium state.
- The surface temperature of solar collectors is constant.
- Solar collectors and other components have a constant heat capacity.

2.6.1. Energy analysis

The first law of thermodynamics can be used for energy analysis, which is a basic performance-evaluation metric.

The solar collector field gathers solar radiation and converts it into useful energy with some energy lost in the environment. Energy conservation equation in the solar collector field can be expressed by Eq. (12):

$$Q_{\text{abs}} = Q_U + Q_L \tag{12}$$

where Q_{abs}, Q_U and Q_L is absorbed energy, useful energy, and loss energy respectively. Incident intensity, concentration ratio, solar collector area, transmission efficiency, optical efficiency and absorption efficiency are all factors that

influence the total amount of solar energy collected in a solar collector field [26] and it can be evaluated using Eq. (13):

$$Q_{\text{abs}} = n \times I \times A_r \times \in \times \alpha \times \tau \tag{13}$$

where I, n, A_r, τ, α and ϵ are direct normal irradiance, concentration ratio, area of receiver, receiver's transmissivity, absorptivity of receiver and optical efficiency of collector respectively.

Convective heat loss and radiative heat loss are two types of energy losses, as illustrated by Eq. (14):

$$Q_L = Q_C + Q_R \tag{14}$$

Convection heat loss and radiation heat loss can be determined respectively by Eqs. (15) and (16) [26,27]:

$$Q_c = h_c \times \left(T_c - T_o\right) \times A \tag{15}$$

$$Q_r = h_r \times \left(T_c - T_o\right) \times A \tag{16}$$

where h_c is the convective heat transfer coefficient and h_r is the radiative heat transfer coefficient. T_C is collector's surface temperature and T_o is the temperature of the environment.

Convective and radiative heat transfer coefficients are calculated by Eqs. (17) and (18), respectively:

$$h_c = 2.8 + 3v \quad 0 < v < 7 \text{m/s} \text{ [28]} \tag{17}$$

$$h_r = \varepsilon \times \sigma \times \frac{\left(T_c^4 - T_{\text{sky}}^4\right)}{\left(T_c - T_{\text{sky}}\right)} \tag{18}$$

where ε is the emissivity, v is the wind velocity and σ is Stefan–Boltzmann constant, T_{sky} is the temperature of an equivalent blackbody.

After calculating absorbed and loss energy, useful energy can be estimated by Eq. (19):

$$Q_u = Q_{\text{abs}} - Q_L \tag{19}$$

Parameters for solar energy calculation are shown in Table 3.

Table 3
Parameters for solar energy calculation

Parameters	Value
Maximum direct normal incidence	1,000 W/m^2
Area of collector	325 m^2
Absorption efficiency of receiver (α)	0.95
Optical efficiency of collector (ε)	0.9
Transmission efficiency of receiver (τ)	0.92
Environment temperature (T_o)	303 K
Sky temperature (T_{sky})	$0.0522 \times T_o^{1.5}$
Stefan Boltzman constant (σ)	5.67×10^{-8} W/m^2·K^4

2.7. Multi-effect distillation process

This model is based on some assumptions such as:

- The feed seawater for each effect is evenly distributed.
- The system's operation is considered to be in steady state.
- The salinity and temperature of the feed seawater are known.
- The BPE (boiling point elevation) is assumed to be constant.
- The entrained vapor and the vapor generated in effects are believed to be saturated.
- Distillate is thought to be salt-free.

Modelling of MED process in ASPEN PLUS software up to seven effects is shown in Fig. 5. Each effect is modeled as a flash and cooler as shown in Fig. 6. Vapors enter the cooler and condense to generate distillate water, which feeds the separator with heat flow Q. This heat can evaporate the incoming seawater feed, generating vapors, which then flows to the second effect, and so on for the next seven effects. The parameters used for modelling and simulation of MED process are shown in Table 4.

2.8. Economic model

This section contains a detailed description of the economic model used in this study. This economic model for the MED setup estimates the capital cost and other operational costs.

2.8.1. Capital cost

A desalination plant's initial investment is equivalent to entire plant's capital cost, which includes costs such as equipment, engineering, erection, commissioning, electronics, control and instrumentation. The MED plants' capital cost is estimated based on the following relation [29]:

$$\text{TCC}_{\text{MED}}\left(\text{US\$}\right) = 3054 \times D_t^{0.9751} \tag{20}$$

where TCC is the MED desalination plant's total capital cost and D_t production rate of MED plant in m^3/d.

2.8.2. Operating expenses

The MED facility's remaining costs are yearly operating expenses. Electrical, maintenance, labour, insurance, and chemical additive expenditures are assumed to make up the annual operating expenses. Operating circumstances, external economic conditions, and reliability of plant are constant over the course of a useful life of MED plant, with an estimated escalation factor to account for inflation in the cost of products and services.

2.8.3. Electricity

Electrical expenses are estimated based on the electricity cost required by all process pumps, which should account for the majority of an MED plant's overall electrical

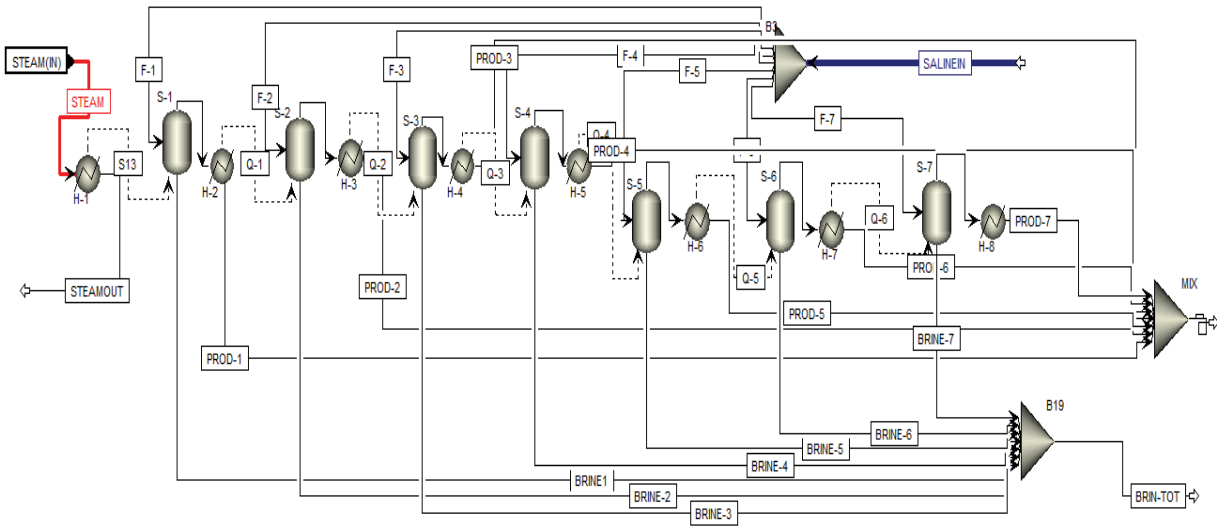

Fig. 5. Modelling of multi-effect distillation process up to 7 effects.

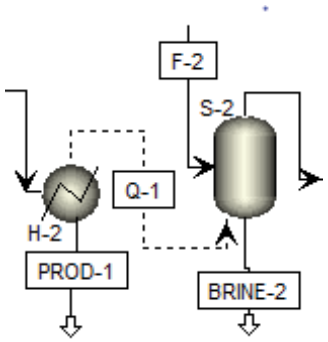

Fig. 6. Modelling of evaporator in ASPEN PLUS® V8.8.

energy usage. Because of existing process simulations, the electricity consumption rate for each process pump is known [29]. The yearly cost of electricity is estimated by Eq. (21):

$$\text{Annual Electrical cost}\left(\frac{\text{US\$}}{\text{yr}}\right)=\text{EUP}\left(\frac{\text{US\$}}{\text{kWh}}\right)\times p\left(\frac{\text{kWh}}{\text{m}^3}\right)\times D_t\left(\frac{\text{m}^3}{\text{day}}\right)\times f\times 365\left(\frac{\text{day}}{\text{yr}}\right) \quad (21)$$

The unit price of electricity (EUP) is supposed to have a cost of Rs. 26/kWh based on Pakistan electricity rates [30], which is equal to 0.168 US$/kWh [31]. The availability of plant "*f*" is supposed to be 95% for each year.

2.8.4. Labour cost

Labor costs are calculated on the basis of actual cost data, with the requirement for one full-time equivalent of qualified employees for every 4,543 m^3/d plant capacity.

Table 4
Parameters for MED process simulation

Parameter		Value
Seawater	Mass flow rate, ton/h	460
	Temperature, °C	28
	Pressure, bar	3
	Salinity, ppm	35,000
Motive steam	Mass flow rate, ton/h	33
	Temperature, °C	305
	Pressure, bar	5
Effects	Temperature S–1, °C	70
	Temperature S–2, °C	63
	Temperature S–3, °C	57
	Temperature S–4, °C	51
	Temperature S–5, °C	45
	Temperature S–6, °C	40
	Temperature S–7, °C	35
	Pressure S–1, bar	0.31
	Pressure S–2, bar	0.23
	Pressure S–3, bar	0.18
	Pressure S–4, bar	0.13
	Pressure S–5, bar	0.1
	Pressure S–6, bar	0.08
	Pressure S–7, bar	0.06
Feed to effects	Mass flow rate, ton/h	65

In Pakistan, the average salary for a worker in the water services industry is 5,779 US$/y [32], so the labour cost is assumed to be set to the specified value and is given by Eq. (22).

$$\text{Labor Cost}_{\text{annual}}\left(\frac{\text{US\$}}{\text{yr}}\right)=5{,}779\left(\frac{\text{US\$}}{\text{yr}}\right) \quad (22)$$

2.8.5. Chemicals cost

Chemical additives are required for the successful and long-term operation of the desalination process and represents a considerable fraction of yearly expense. Based upon values from literature [33–35], the cost of chemical dosing in MED feed is assumed as 0.0223 US$/m^3, and the specific cost of chemical in evaporator is assumed as 0.0198 US$/m^3 [33,35,36], supposing that the chemical needs of the flashing chamber feed are identical to those of MED system evaporators at low temperatures.

2.8.6. Maintenance and insurance cost

The yearly cost of insurance and maintenance activities is supposed to be 1.5% of the plant's total capital cost [37] as expressed in Eq. (23). The cost of spares and maintenance for any MED plant is significantly influenced by management expertise, cash flow timing and engineering services. However, in the absence of a viable alternative, such expenses are calculated as a proportion of the entire capital cost of the plant.

$$\text{Maintenance and Insurance cost}\left(\frac{\text{US\$}}{\text{yr}}\right)=1.5\%\times\text{TCC} \tag{23}$$

Here the plant's total capital cost (TCC), is calculated as a function of production capacity as described in section 2.6.1.

2.8.7. Incomes

It is assumed that the MED plant's earnings over a given time are equal to the earnings generated from the drinking water whose volume is equal to the plant's total production over that time, sold at the average price in the market.

$$\text{Income}=365\times D_t\left(\frac{\text{m}^3}{\text{day}}\right)\times f\times\text{WMP}\left(\frac{\text{US\$}}{\text{m}^3}\right) \tag{24}$$

Here, WMP is the distillate market price available from a supplier which is the average price of water in Pakistan of 11.6 US$/m^3 [38]. The income for the following years is calculated using a 3% escalation rate.

3. Results and discussion

3.1. Validation of models

The simulation models of gas turbine, heat recovery steam generator and MED, developed in the ASPEN PLUS were validated with the literature data as presented in upcoming subsections.

3.1.1. Gas turbine

The gas turbine simulation model developed in ASPEN PLUS is validated with the results of Promes et al. [39] as shown in Fig. 7. The simulation results of gas turbine model are in agreement with the literature data with negligible error which can be seen from Table 5.

3.1.1. Heat recovery steam generator

The HRSG simulation model developed in ASPEN PLUS is validated with the results of Olivieri and Ravelli [40]. The simulation results of HRSG model are in agreement with the literature data with negligible error which can be seen from Table 6.

3.1.2. MED model

The MED simulation model developed in ASPEN PLUS is validated with the results of Maha et al. [41]. The simulation results of MED model are in agreement with the literature data with negligible error which can be seen from Table 7.

3.2. Effect of operating parameters on GOR

3.2.1. Number of MED effects

The number of MED effects are very important to keep the balance between cost and amount of distillate produced in the MED system. The influence of increasing number of effects on GOR is shown in Fig. 8. GOR was calculated for effects ranging from 1 to 9.

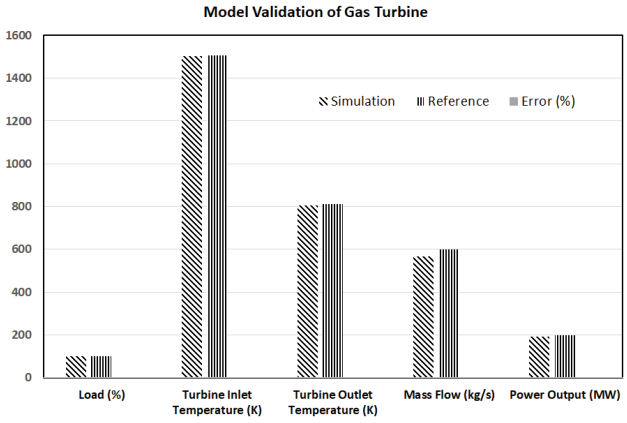

Fig. 7. Validation of parameters in gas turbine.

Table 5
Validation of parameters in gas turbine

Parameters	Simulation	Reference	Error (%)
Load (%)	100	100	0
Turbine inlet temperature (K)	1,503	1,505	–0.13307
Turbine outlet temperature (K)	804.9	810	–0.63362
Mass flow (kg/s)	567	599	–5.64374
Power output (MW)	192	199	–3.64583

Table 6
Validation of parameters in heat recovery steam generator

Parameters	Simulation	Reference	Error (%)
HP steam turbine inlet pressure (bar)	101	100.8	0.19802
HP steam turbine outlet pressure (bar)	28	28	0
HP turbine inlet temperature (°C)	505	503.7	0.25743
HP turbine outlet temperature (°C)	335.6	327.8	2.3242
HP steam mass flow (kg/s)	77	77.1	0.1297
IP steam turbine inlet pressure (bar)	27	26.8	0.74074
IP steam turbine outlet pressure (bar)	3.2	3.2	0
IP turbine inlet temperature (°C)	490	490	0
IP turbine outlet temperature (°C)	230.2	227	1.3901
IP steam mass flow (kg/s)	88.5	88.4	0.11299
LP steam turbine inlet pressure (bar)	3.2	3.4	–6.25
Net power output (MW)	252.4	240.2	4.833597

Table 7
Validation of MED model

Parameters	Simulation	Reference	Error (%)
Driving vapor pressure (bar)	5	5	0
Seawater for one cell (ton/h)	20	20	0
Heating vapor in first effect (ton/h)	6.43	6.43	0
First effect temperature (°C)	60.3	60	0.5
Second effect temperature (°C)	50.2	50	0.4
Third effect temperature (°C)	40.8	40	2
Total production (ton/h)	18.7	19.4	3.6

GOR increases from 0.52 for the first effect to 8.62 for the ninth. It was observed that GOR increased from 7.46 to 8.13 for the seventh to eighth effect and from 8.13 to 8.62 for the eighth to ninth effect. It can be inferred from these values that GOR increased with increase in number of effects. However, slope of line decreased and GOR didn't increase considerably after seventh effect. Hence, increasing number of effects greater than 7 was not feasible from economic point of view. More distillate product can be produced with increase in number of effects. According to literature, the main reason of this behavior is that the produced vapors are reused in the next effect/stage which ultimately increase the output of MED plant. However, higher number of MED effects lead to higher capital cost resulting in higher distillate cost.

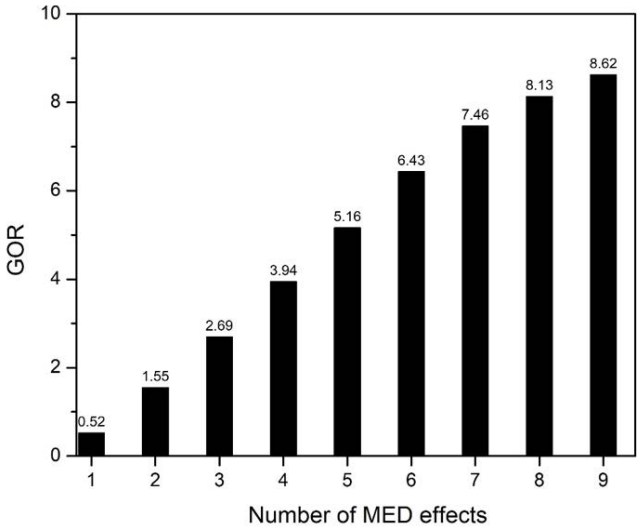

Fig. 8. Impact of number of MED effects on GOR.

3.2.2. Heat input

Fig. 9 illustrates the influence of heat input on GOR for different number of MED effects. Heat input in the first effect of MED was a major factor affecting GOR. Increasing heat input in the first effect of MED increased GOR up to a certain level and then it became constant. It could be observed that by increasing the heat input in first effect of MED from 8 to 80 MW, GOR increased from 2.1 to 8.9 for 7 effects, from 1.8 to 8.7 for 6 effects, from 1.7 to 8.4 for 5 effects, from 1.5 to 7.9 for 4 effects and from 1.3 to 7.1 for 3 effects and then became constant. The maximum value of GOR was 8.9 for 7 effects which was achieved at heat input of 32 MW, 8.7 for 6 effects (at heat input of 36 MW), 8.4 for 5 effects (at heat input of 44 MW), 7.9 for 4 effects (at heat input of 56 MW) and 7.1 for 3 effects (at heat input of 72 MW). It can be inferred that higher value of GOR can be achieved with less heat input for higher number of effects. Increasing heat input will result in more distillate produced which will increase GOR but GOR became constant after achieving maximum value for each number of effect. It is due to the constant seawater feed of 460 ton/h that limits GOR from continuously increasing. If seawater feed is not taken as constant and both heat input and seawater feed flow rate are increased, GOR will continuously keep on increasing.

3.2.3. Top brine temperature

The steam heats the seawater to a temperature which is called as top brine temperature (TBT). The effect of TBT

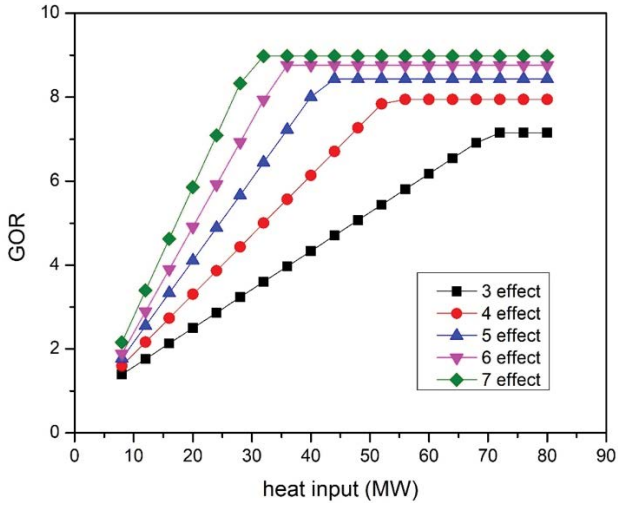

Fig. 9. Effect of heat input (in first effect) on GOR at different number of stages with seawater feed of 460 ton/h.

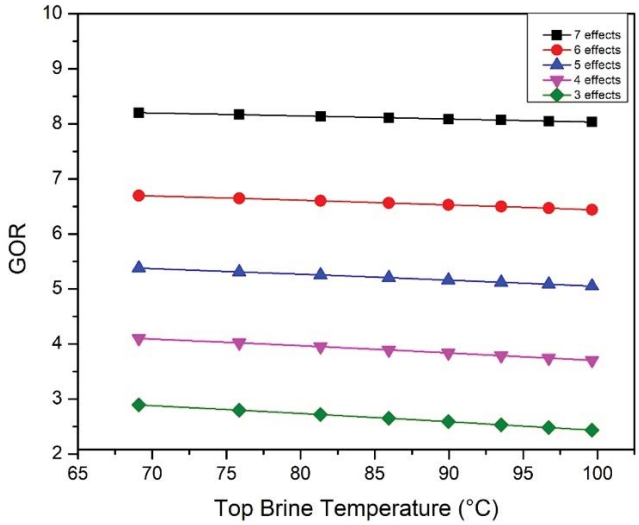

Fig. 10. Effect of top brine temperature (°C) on GOR at different number of stages with seawater feed of 460 ton/h.

on GOR for different number of MED effects is shown in Fig. 10. In this section, TBT was varied from 67°C to 100°C for number of effects ranging from three to seven while seawater feed is constant at 460 ton/h. It could be observed that by increasing the TBT from 67°C to 95°C, GOR reduces from 8.2 to 8 for 7 effects, from 6.7 to 6.4 for 6 effects, from 5.4 to 5 for 5 effects, from 4.1 to 3.7 for 4 effects and from 2.9 to 2.4 for 3 effects. The peak value of GOR occurred for lower TBT and higher number of effects. Therefore, there was a slight decrease in GOR by increasing the TBT for different number of MED effects. According to literature, the main reason of this behavior is that when the TBT increases, the vapor latent heat decreases and the amount of feed sensible heating increases which results in decrease of GOR.

3.3. Influence of feed salinity

3.3.1. GOR

The influence of feed salinity on GOR is shown in Fig. 11 for different number of MED effects. On average, the world's seawater has a salt concentration of about 3.5% (35 g/L) which means that one kg of seawater has about 35 g of dissolved salts. In the present study, feed water salinity is varied starting from 0.5% to 5% for number of effects ranging from three to seven while seawater feed is constant at 460 ton/h. It was observed that when feed water concentration was increased from 0.5% to 5%, GOR reduced from 8.2 to 5.4 for 7 effects, from 6.5 to 4.5 for 6 effects, from 5.2 to 3.6 for 5 effects, from 4.2 to 2.6 for 4 effects and from 2.9 to 1.1 for 3 effects. The peak value of GOR occurred for 7 effects and pure water. Therefore, there is a considerable decrease in GOR by increasing the feed salinity irrespective of the number of effects. The fundamental explanation for this influence is that when feed salinity increases, viscosity rises as well, lowering the thermal conductivity and diffusion rate of the feed solution. Moreover, the amount of fresh water produced, and secondary steam generated by each effect is reduced. Furthermore, the impact of the

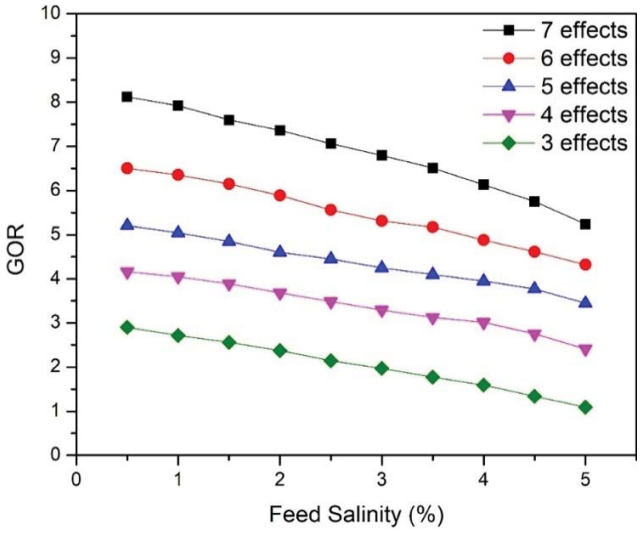

Fig. 11. Influence of feed salinity on GOR at different number of stages with seawater feed of 460 ton/h.

BPE (boiling point elevation) is increased with the salinity. Consequently, the temperature difference increases with the number of effects and heat transfer performance decreases. As a result, the system's thermal efficiency is lowered, resulting in greater steam consumption and lower GOR.

3.3.1. Total heat transfer area of MED

The influence of feed salinity on total heat transfer area is shown in Fig. 12 for different number of effects.

The salinity of feed water was varied from 0.5% to 5% for number of effects ranging from three to seven while seawater feed was constant at 460 ton/h. It could be observed that by increasing the feed saltwater concentration from

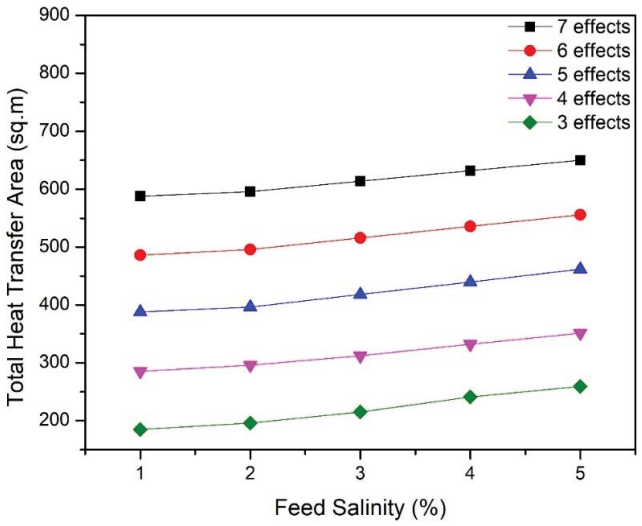

Fig. 12. Influence of feed salinity on total heat transfer area (m^2) at different number of stages with seawater feed of 460 ton/h.

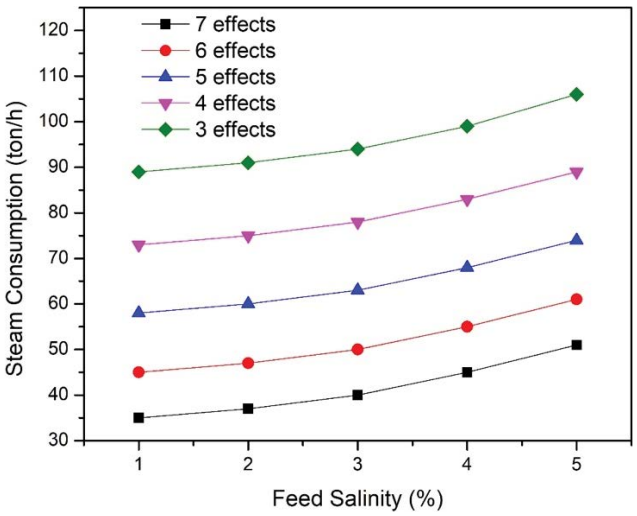

Fig. 13. Influence of feed salinity on steam consumption (ton/h) at different number of stages with seawater feed of 460 ton/h.

0.5% to 5%, total heat transfer area increases from 588 to 650 m^2 for 7 effects, from 486 to 556 m^2 for 6 effects, from 388 to 462 m^2 for 5 effects, from 285 to 351 m^2 for 4 effects and from 185 to 259 m^2 for 3 effects. Therefore, there is a trivial rise in total heat transfer area by increasing the feed salinity for different effect numbers. Because each effect's concentration rises with feed salinity, that depicted a positive correlation between feed salinity and heat transfer area of the evaporator. As a result, the loss of heat transfer temperature difference induced by boiling point elevation rises which results in a decrease in the temperature differential between adjacent effects, as well as a decrease in each effect's evaporation capacity, leading to an increase in total heat transfer areas.

3.3.2. Steam consumption

The dependence of feed salinity on steam consumption (ton/h) is shown in Fig. 13 for different number of MED effects. In this study, the salinity of feed water was varied from 0.5% to 5% for number of effects ranging from three to seven while seawater feed is constant at 460 ton/h. It could be observed that by increasing the feed saltwater concentration from 0.5% to 5%, steam consumption increased from 35 to 51 ton/h for 7 effects, from 45 to 61 ton/h for 6 effects, from 58 to 74 ton/h for 5 effects, from 73 to 89 ton/h for 4 effects and from 89 to 106 ton/h for 3 effects. The peak value of steam consumption occurred for pure water and 7 effects. Therefore, there is a considerable increase in steam consumption by increasing the feed salinity for different number of effects. This behavior is in accordance with the literature. The reasonable explanation according to literature for this behavior is that the viscosity of the feed solution rise with the feed salinity, which is followed by a decrease in the diffusion coefficient and thermal conductivity of the feed solution. At the same time, the amount of distillate and secondary steam produced by each effect decreases. The impact of the boiling point elevation (BPE) is also increased when the salinity is increased. As a result

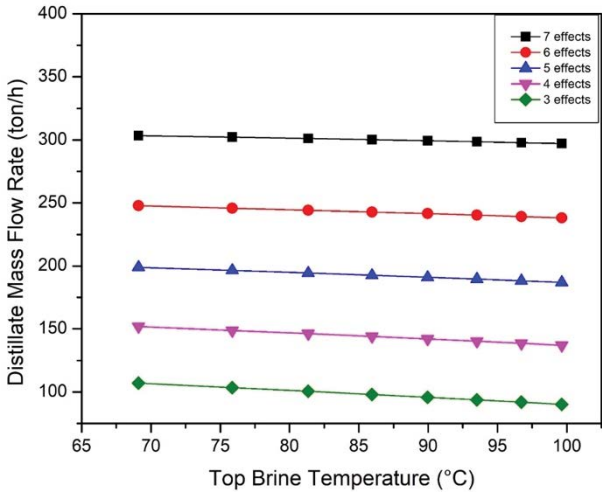

Fig. 14. Effect of top brine temperature (°C) on distillate produced (ton/h) at different number of stages with seawater feed of 460 ton/h.

of the effect numbers, the effective heat transfer temperature difference increases, and heat transfer efficiency falls resulting in a decreased system's thermal efficiency which ultimately results in higher steam usage as well as lower GOR.

3.4. Effect of top brine temperature on distillate production

The effect of TBT on distillate produced (ton/h) is shown in Fig. 14 for different number of effects. In this section, TBT was varied from 68°C to 98°C for number of effects ranging from three to seven while seawater feed was constant at 460 ton/h. It could be observed that by increasing the TBT from 68°C to 98°C, distillate flow rate decreased from 303 to 297 ton/h for 7 effects, from 247 to 238 ton/h for 6 effects, from 199 to 186 ton/h for 5

effects, from 151 to 137 ton/h for 4 effects and from 107 to 90 ton/h for 3 effects. The peak value of distillate produced occurred for lower TBT and higher effect number. Therefore, there is a decrease in distillate produced by increasing the top brine temperature for different number of effects. As GOR is decreasing with increase in TBT, distillate flow rate will also have decreasing trend as distillate produced is directly linked with GOR.

3.5. Dependence of evaporator pressure on distillate production

MED operates at a pressure lower than the atmospheric (vacuum pressure) so distillate produced in a particular effect strongly depends on the pressure in that evaporator. The dependence of effect pressure on distillate production (ton/h) in first effect is shown in Fig. 15. In this section, pressure in first effect was varied from 0.1 bar to 1 bar for number of effects ranging from three to seven while seawater feed was constant at 460 ton/h. It could be observed that by increasing the effect pressure from 0.1 bar to 1 bar, distillate production in first effect decreased from 44 to 42 ton/h for 7 effects, from 44 to 39 ton/h for 6 effects, from 43 to 37 ton/h for 5 effects, from 42 to 34 ton/h for 4 effects and from 41 to 30 ton/h for 3 effects. The peak value of distillate flow rate in the first stage of MED occurred at lower pressure and higher number of effects. Therefore, distillate production decreased by increasing the pressure in first effect for different number of effects. The decrease in distillate production with increase in pressure is of considerable importance for lesser number of effects as compared to higher number of effects. The dependence of effect pressure on distillate production (ton/h) in second and third effect is shown in Figs. 16 and 17. Same trend as first effect was observed for second and third effect. This result is in exact accordance with the literature as lower pressure results in reduced boiling temperature and less energy is required in order to produce a desired amount of distillate. Increasing the pressure in effects will also increase the boiling point of water and the production of distillate will continuously decrease.

3.6. Effect of mass flow rate of seawater feed on distillate production

The effect of mass flow rate of seawater feed on distillate production (ton/h) is shown in Fig. 18 for different number of MED effects. In this section, the mass flow rate of seawater feed was varied from 150 to 510 ton/h for number of effects ranging from four to seven while steam flow rate was constant at 37 ton/h. It could be observed that by increasing the mass flow rate of seawater feed from 150 to 510 ton/h, distillate flow rate increased from 128 to 177 ton/h and then decreased to 158 ton/h for 4 effects, increased from 128 to 220 ton/h and then decreased to 192 ton/h for 5

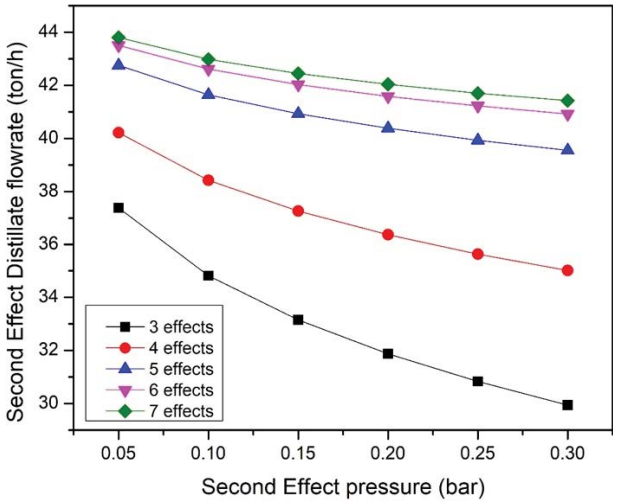

Fig. 16. Dependence of pressure on distillate production (ton/h) in second stage for different number of MED effects, seawater feed constant at 460 ton/h.

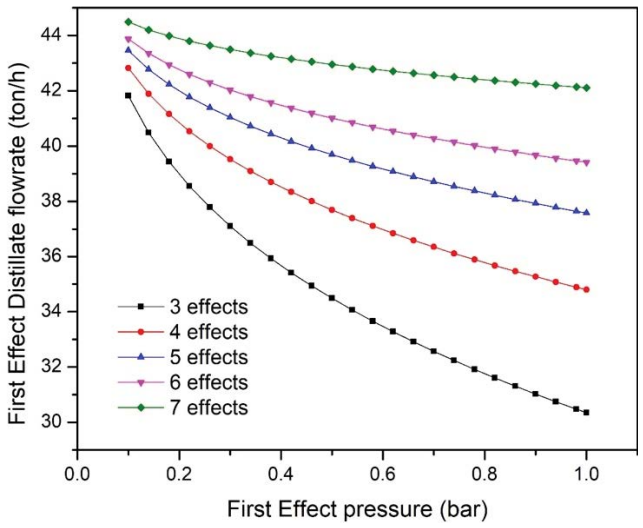

Fig. 15. Dependence of pressure on distillate production (ton/h) in first stage for different number of MED effects, seawater feed constant at 460 ton/h.

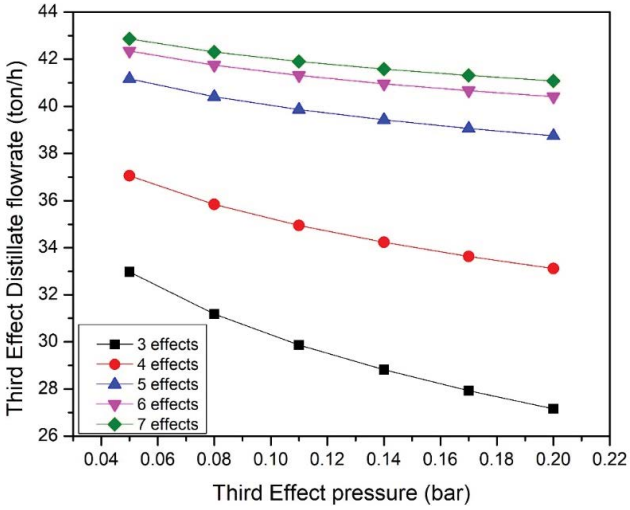

Fig. 17. Dependence of pressure on distillate production (ton/h) in third stage for different number of MED effects, seawater feed constant at 460 ton/h.

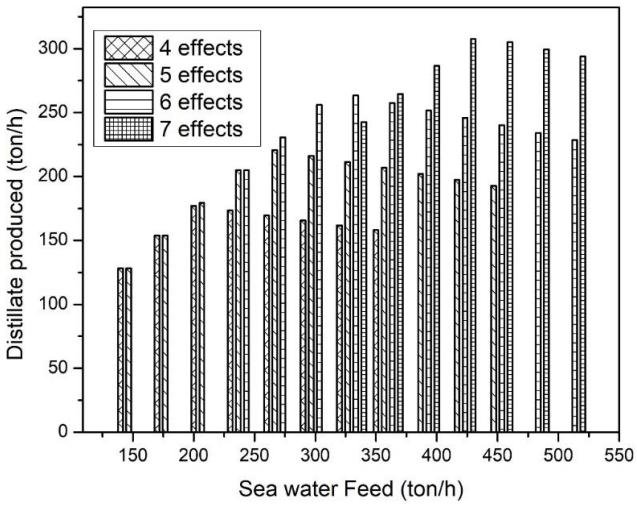

Fig. 18. Effect of mass flow rate of seawater feed on distillate production at constant seawater feed temperature of 28°C.

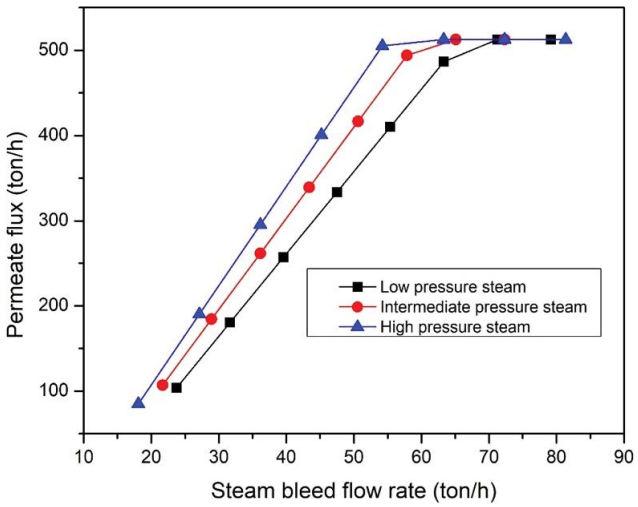

Fig. 19. Effect of steam bleed flow rate (ton/h) in CCP on permeate flux (ton/h) with seawater feed of 600 ton/h.

effects, increased from 204 to 263 ton/h and then decreased to 228 ton/h for 6 effects, increased from 242 to 307 ton/h and then decreased to 293 ton/h for 7 effects. The peak value of distillate flow rate was achieved at higher number of effects. Therefore, increase in mass flow rate of seawater feed results in an increased distillate production and after reaching maximum value, it starts to decrease.

The results were further validated by comparing them with the literature. Rahimi et al. [42] studied the behavior of increasing MED effects with GOR at different steam pressure and found out similar results showing increase of GOR with increase in number of MED effects. Karim et al. [43] studied the effect of increase in feed salinity on GOR and found that increase in feed salinity results in drop of GOR which validate our results. Xue et al. [44] developed a mathematical model on basis of mass and energy balance to study the effect of various parameters on total heat transfer area and steam consumption. It was concluded that increase of feed salinity results in increase in both heat transfer area and steam consumption which is in accordance with our findings.

3.7. Coupling of combined cycle power plant with MED

After producing power in gas turbine section, hot gases were then fed into steam generation portion of combined cycle power plant where these hot gases exchange heat with water to produce steam. This produced steam was classified as high-pressure, low-pressure and intermediate pressure steam, running the high-pressure, low-pressure and intermediate pressure turbines, respectively. These different pressure streams were bled before entering the turbines and were introduced in first effect of MED to heat up the incoming feed water.

3.7.1. Effect of bleed steam flow rate on permeate flux produced

Three different pressure streams of steam produced in steam generation portion of combined cycle power plant were separately introduced in MED first effect and their dependence on permeate flux produced was observed as is shown in Fig. 19. In this study, the flow rate of these different pressure steams was varied from 18 to 82 ton/h while seawater feed was constant at 600 ton/h with seven stages. It could be observed that by increasing the flow rate of these streams from 18 to 82 ton/h, permeate flux increased from 85 to 512 ton/h and then became constant for high-pressure steam, increased from 106 to 512 ton/h and then became constant for intermediate pressure steam, increased from 103 to 512 ton/h and then became constant for low-pressure steam.

A constant permeate flux of 512 ton/h was achieved from 53 ton/h of high-pressure steam, 65 ton/h of intermediate pressure steam and 72 ton/h of low-pressure steam. Increasing steam flow rate beyond this was of no use as it didn't increase permeate flux (it was limited by seawater feed flow rate).

Now, in addition to keeping seawater feed constant at 600 ton/h and number of effects at 7, permeate flux was also kept constant at 500 ton/h and bleed flow rate of different pressure steam was determined. It could be observed from Fig. 20 that permeate flux of 500 ton/h was produced in MED when high-pressure steam at 53.69 ton/h, intermediate pressure steam at 58.43 ton/h and low-pressure steam at 64.74 ton/h were introduced separately in first effect of MED. Meanwhile, power output produced after bleeding high-pressure steam of 53.69 ton/h was 127.15 MW, bleeding intermediate pressure steam of 58.43 ton/h was 126.42 MW and bleeding low-pressure steam of 64.74 ton/h was 128.13 MW. It can be concluded that less flow rate of high-pressure steam is required in first MED to produce constant flux as compared to intermediate and low-pressure steam.

3.7.2. Effect of bleed steam flow rate on power output

As discussed earlier, three different pressure streams of steam produced in steam generation portion of combined

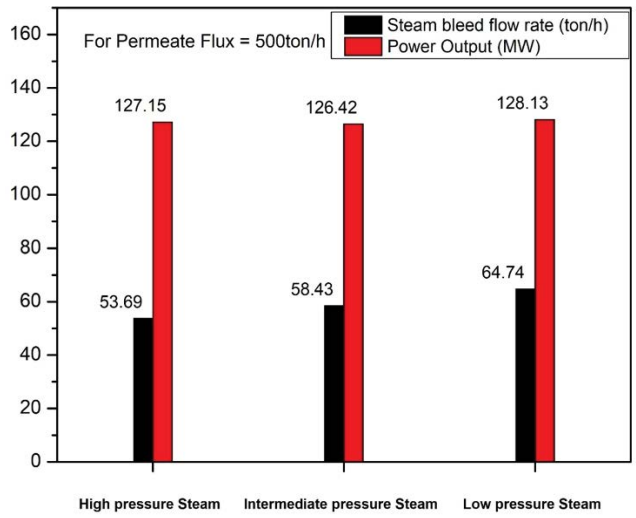

Fig. 20. Effect of steam bleed flow rate (ton/h) on permeate flux (ton/h) and power output (MW) of CCP at seawater feed of 600 ton/h.

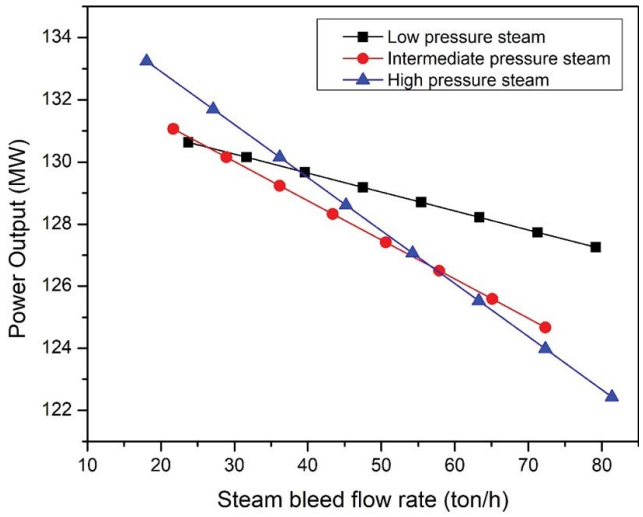

Fig. 21. Effect of steam bleed flow rate (ton/h) in CCP on power output (MW) at seawater feed of 600 ton/h.

cycle power plant were separately introduced in MED first effect. This bleeding of steam has considerable effect on power output in CCP. This dependence of steam flow rate on power output is plotted in Fig. 21. In this study, the flow rate of these different pressure steam was varied from 18 to 82 ton/h while seawater feed was constant at 600 ton/h and number of effects are kept constant at 7. It could be observed that by increasing the bleeding stream flow rate from 18 to 82 ton/h, power output decreased from 133 to 122 MW for high-pressure steam, decreased from 131 to 124 MW for intermediate pressure steam and decreased from 130 to 127 MW for low-pressure steam. The drop in power output was 11 MW for high-pressure steam, 7 MW for intermediate pressure steam and 3 MW for low-pressure steam. So, it is concluded that more drop in power output occurred while bleeding high-pressure

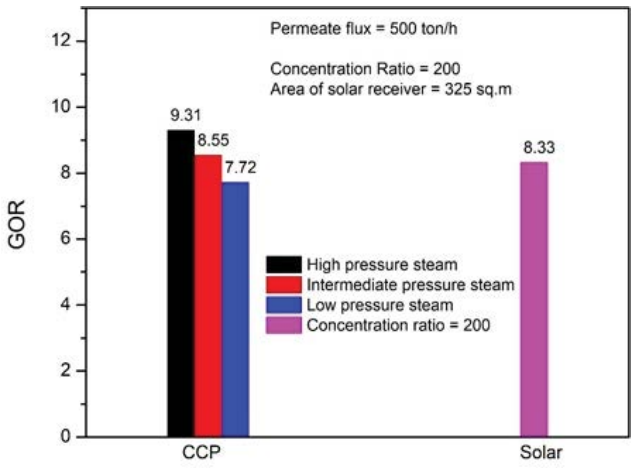

Fig. 22. Comparison of CCP-MED with solar-MED.

steam and drop in power output was least when low-pressure steam was bled. However, from previous section, it was concluded that less flow rate of high-pressure steam was needed to produce a constant permeate flux as compared to low-pressure steam, so bleeding intermediate pressure steam is a feasible option.

3.8. Comparison of CCP and solar energy coupled with MED

Fig. 22 shows the comparison between combined cycle power plant and solar energy when coupled with MED plant. Saline feed was fixed at 600 ton/h and permeate flux was also kept constant at 350 ton/h. GOR was calculated for 3 different pressure streams, that is, high-pressure (HP), low-pressure (LP) and intermediate pressure steam (IP) and it was also calculated for solar energy. GOR comes out to be 9.31 (HP), 8.55 (IP), 7.72 (LP) and 8.33 when solar energy was coupled with MED. Highest value of GOR was achieved for bleeding high-pressure steam, however, this high GOR comes out at the cost of lower power output in CCP, while lowest value of GOR was achieved while bleeding LP steam. It can be further deduced that in order to achieve 350 ton/h of permeate flux, a concentration ratio of 200 and an area of collector of 325 m^2 is the minimum requirement in case of solar energy coupled with MED. Concentration ratio of 200 can be achieved by using parabolic dish reflector. Obviously, permeate flux can be increased with more concentration ratio and larger area of collector as it will increase the heat available for MED process.

3.9. Impact of variable solar flux on permeate production

Fig. 23 shows the impact of direct normal irradiance on heat available from solar collector and distillate flow rate for seven stages at constant steam flow rate of 20 ton/h. Solar flux was varied from 300 to 1,000 W/m^2 and it was observed that heat available from solar collector increased which ultimately resulted in higher permeate flux.

3.10. Exergy analysis

Calculations of system exergy losses and irreversibility give helpful information for locating the units responsible

for these losses and energy consumption. Exergy destruction in different MED effects is shown in Fig. 24. It was calculated for different effects ranging from one to seven. The exergy destruction decreased from 781 in first effect to 227 in seventh effect. Exergy destruction for second effect was 781 kW, for third effect was 608 kW, for fourth effect was 520 kW, for fifth effect was 373 kW, for sixth effect was 304 kW and for seventh effect was 227 kW. Thus exergy destruction decreased as we moved across the effects. Increasing number of effects resulted in lower exergy destruction. The main reason was that by increasing effect number, temperature drop per effect decreased which resulted in less irreversibility and thus less exergy destruction.

Exergy destruction in different MED effects with their respective temperatures is shown in Fig. 25. It shows that exergy destruction in second effect at temperature of 60°C was 781 kW, in third effect at temperature of 52°C was 608 kW, in fourth effect at temperature of 45°C was 520 kW, in fifth effect at temperature of 40°C was 373 kW, in sixth effect at temperature of 36°C was 304 kW and in seventh effect at temperature of 33°C was 227 kW. Exergy destruction was more for second effect with higher temperature as compared to seventh effect which was at lower temperature. So it can be deduced that while progressing from higher temperature effects to lower temperature effects, exergy destruction decreased.

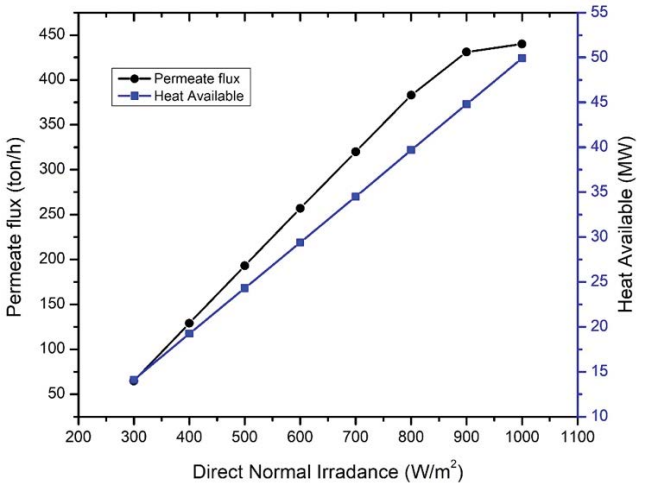

Fig. 23. Impact of variable solar flux on permeate production and heat available from solar collector at concentration ratio of 200 and solar collector area of 325 m^2.

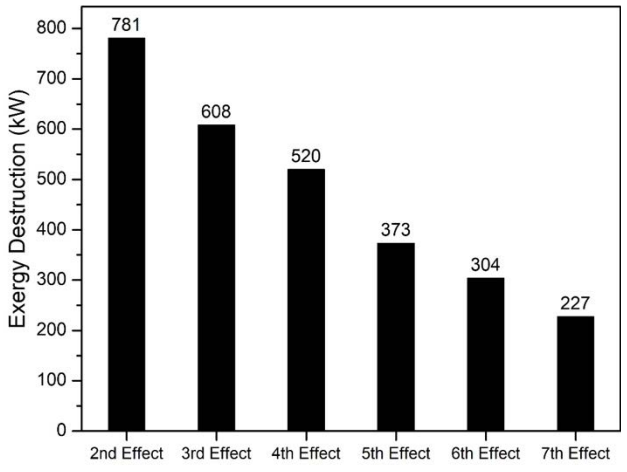

Fig. 24. Exergy destruction in different MED stages.

3.11. Economic analysis

3.11.1. Cost distribution

In this section, economic analysis of MED plant coupled with both solar energy and combined cycle power plant is discussed. Table 8 shows the cost distribution of MED plant coupled with solar energy. Cost distribution mainly consists of capital cost, steam cost, electricity cost, maintenance and insurance cost, labor cost and chemical cost. Capital cost constituted 74.2%, steam 21.8%, electricity 2.1%, maintenance and insurance 1.1%, labor 0.3% and chemical cost constitutes 0.2% of total cost. Hence, major cost was the capital cost of MED plant followed by cost of steam production from solar energy. All costs are in dollars per year except capital cost (in USD for one time).

Table 9 shows the cost distribution when MED plant is coupled with combined cycle power plant. It can be inferred that cost distribution mainly consists of capital cost, steam

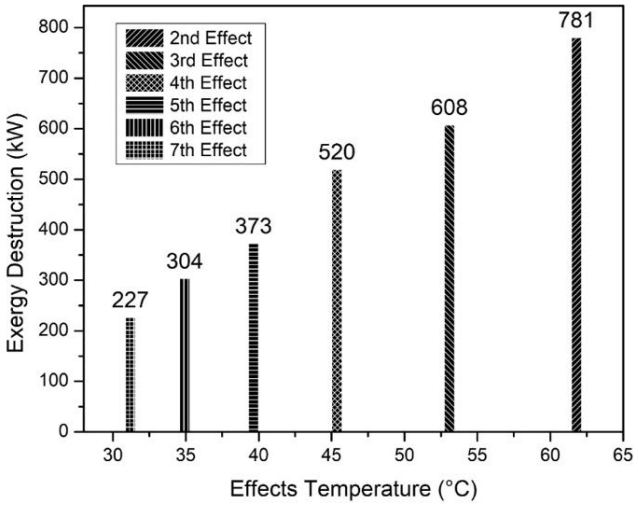

Fig. 25. Exergy destruction w.r.t effects temperature.

Table 8
Cost distribution for MED-solar coupling

Type of costs	Percentage (%)
Total capital cost ($)	74.2
Steam cost ($/y)	21.8
Electricity cost ($/y)	2.1
Maintenance and insurance cost ($/y)	1.1
Labor cost ($/y)	0.3
Chemical cost ($/y)	0.2

cost, electricity cost, maintenance and insurance cost, labor cost and chemical cost. Capital cost constituted 79.9%, steam 15.9%, electricity 2.2%, maintenance and insurance 1.1%, labor 0.4% and chemical 0.2% of total cost. Capital cost was the main cost followed by steam obtained from combined cycle power plant. From this data, it can be seen that steam cost from CCP was 15.9% of total while the steam cost in case of solar energy was 21.8%. Hence, it can be deduced that cost of steam from combined cycle power plant is less as compared to solar energy.

3.11.2. Effect of MED capacity on different cost types

3.11.2.1. Total capital cost

The effect of MED capacity (m^3/d) on total capital cost ($) is shown in Fig. 26. In this analysis, the MED capacity was varied from 4,000 to 9,000 m^3/d. It could be observed that by increasing the MED capacity, total capital cost increased from 10 to 22 M$. Therefore, capital cost increased by increasing MED capacity because a direct relation exists between them.

3.11.2.2. Operation cost

The effect of MED capacity (m^3/d) on operational cost ($) in case of MED coupled with both solar energy and CCP is shown in Fig. 27. It could be observed that by increasing the MED capacity, the operational cost increased from 3.1 to 5.6 M$ for CCP and increased from 4.3 to 7.7 M$ for solar energy. Hence, overall the operational cost of solar energy was more than that of CCP.

3.11.2.3. Production cost

The effect of MED capacity (m^3/d) on production cost ($) in case of MED coupled with both solar energy and CCP is shown in Fig. 28. In this analysis, the MED capacity is varied from 4,000 to 9,000 m^3/d. It could be observed that by increasing the MED capacity, production cost increased from 13 to 29 M$ for CCP and increased from 15 to 31 M$ for solar energy. So again, the production cost of solar energy was more than that of CCP.

Table 9
Cost distribution for MED-CCP coupling

Type of costs	Percentage (%)
Total capital cost ($)	79.9
Steam cost ($/y)	15.9
Electricity cost ($/y)	2.2
Maintenance and insurance cost ($/y)	1.1
Labor cost ($/y)	0.4
Chemical cost ($/y)	0.2

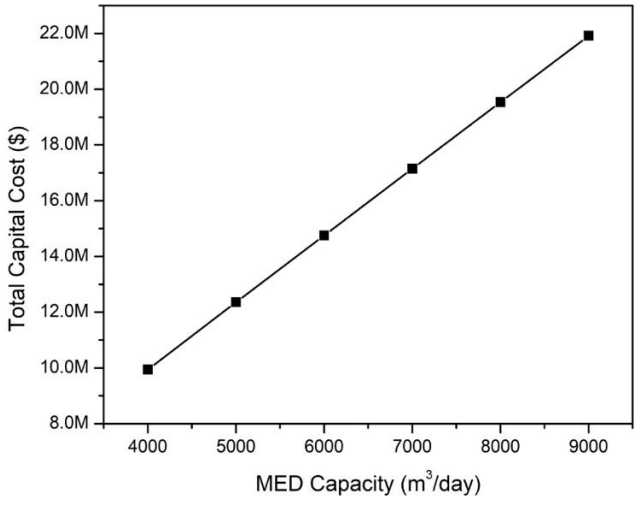

Fig. 26. Effect of MED capacity on total capital cost.

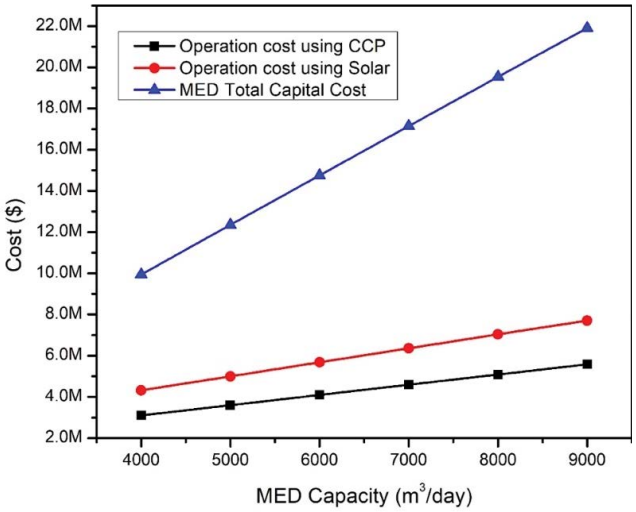

Fig. 27. Effect of MED capacity ranging from 4,000 to 9,000 m^3/d on total capital cost and operation cost using both CCP and solar energy.

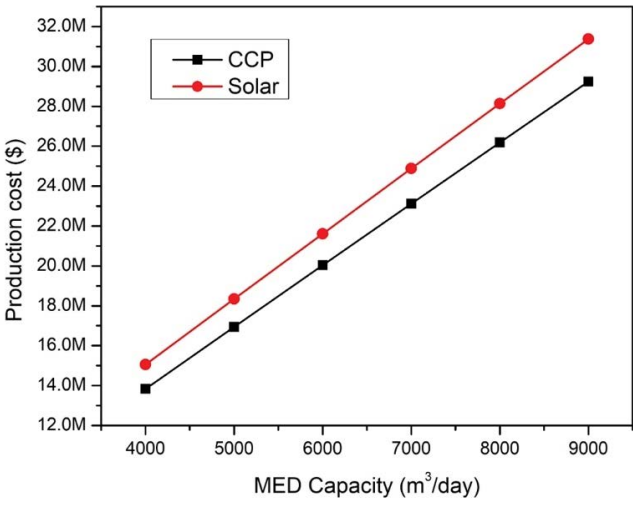

Fig. 28. Effect of MED capacity ranging from 4,000 to 9,000 m^3/d on production cost.

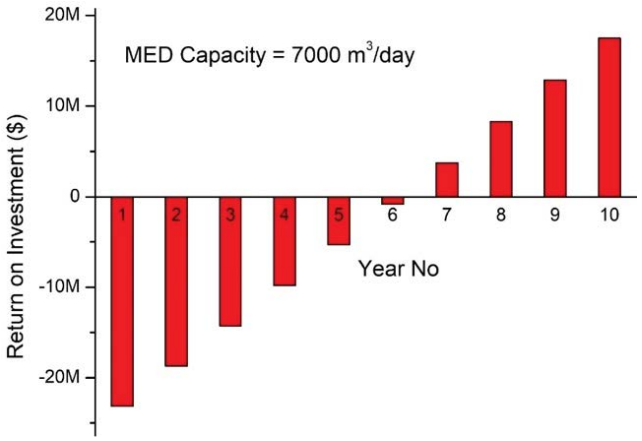

Fig. 29. Return on investment for MED plant having capacity of 7,000 m³/d.

3.11.3. Return on investment

The return on investment of an MED process is shown in Fig. 29. Firstly, investment was done on MED process which mainly consists of capital cost and some other costs. It took some time to balance out the investment and then it started generating revenue. After calculating income and initial investment, return on investment was evaluated and then finally plotted. In initial years, ROI was negative as the initial investment hasn't been recovered. It took approximately 6 y for MED plant having capacity of 7,000 m³/d to balance out the investment and ROI started after 6 y.

The demand for clean energy is high and the transition from fossil fuel-based energy to environmentally friendly sources is the next stage in eliminating global greenhouse gas (GHG) emissions. One of the most promising technologies for producing low-carbon, non-fossil fuel energy has been solar energy. On the other hand, cogeneration systems are a green choice for energy production if biogas or other renewable fuels are used as their main fuels. But the system is not an eco-friendly choice if it runs on diesel or other fossil fuels.

4. Conclusions

In this present work, parametric study of MED and comparison of both combinations MED-CCP and MED-solar was carried out by performing simulation in ASPEN PLUS® V8.8. The impact of various crucial process parameters like number of MED effects, top brine temperature (TBT), feed salinity and heat input on gain output ratio were investigated and the effect of change in feed salinity on total heat transfer area and steam consumption were explored. In addition, exergetic analysis for MED process and economic analysis for both combinations MED-CCP and MED-solar was performed. Following are the important conclusions drawn from the study.

- The effect numbers are very important to keep the balance between lower costs and more distillate product in the MED system. With increase in effect numbers, more distillate product can be produced. However higher effect numbers lead to higher capital cost and distillate product cost.
- In addition, increasing feed salinity promotes the total heat transfer areas and increases steam consumption resulting in reduction of GOR.
- As we increase heat input in first effect of MED, GOR first increased and then became constant for each effect. Also, increase in TBT slightly decreased both GOR and distillate product.
- Increase in effect pressure of first effect decreased distillate product.
- Less flow rate of high-pressure steam was required in CCP to achieve a desired distillate product (high GOR) as compared to low-pressure steam but power output drops considerably when bleeding high-pressure steam, so intermediate pressure steam is recommended for bleeding.
- In order to achieve same amount of distillate product from CCP and solar, high concentration ratio and more area of collector was required in case of solar energy which makes CCP process more economically feasible.
- Exergy destruction progressively decreased while moving towards the higher effects. Effects with high temperature have more exergy destruction as compared to lower temperature effects.
- Capital cost, operation cost and production cost increased with increase in MED capacity. These costs were higher for solar energy as compared to CCP because the cost of steam which is obtained from solar collectors was more than CCP.
- Return on investment comes out approximately 6 y for fix MED capacity of 7,000 m³/d.

Abbreviations

BPE	—	Boiling point elevation
CCPC	—	Combined cycle power cycle
CCPP	—	Combined cycle power plant
CHP	—	Combined heat and power
CRGT	—	Chemically recuperated gas turbine
CSP	—	Concentrated solar power
EES	—	Engineering equation solver
EUP	—	Electricity unit price
FPC	—	Flat plate collector
GOR	—	Gain output ratio
HRSG	—	Heat recovery steam generator
HTF	—	Heat transfer fluid
IRR	—	Internal rate of return
LT-MED	—	Low-temperature multi-effect distillation
MD	—	Membrane distillation
MED	—	Multi-effect distillation
MSF	—	Multi stage flash distillation
NEA	—	Non-equilibrium allowance
NPV	—	Net present value
ORC	—	Organic Rankine cycle
PDE	—	Partial differential equation
PTC	—	Parabolic trough collector
PTFE	—	Polytetrafluoroethylene
PV	—	Photo-voltaic
RO	—	Reverse osmosis
ROI	—	Return on investment

TBT	—	Top brine temperature
TCC	—	Total capital cost
TVC	—	Thermal vapor compression
VC	—	Vapor compression

Symbols

A_r	—	Receiver area, m^2
D_t	—	Total production rate, m^3/d
f	—	Plant availability, %
H	—	Enthalpy, kJ
h	—	Specific enthalpy, kJ/kg
h_c	—	Convective heat transfer coefficient, $W/m^2 \cdot K$
h_r	—	Radiation heat transfer coefficient, $W/m^2 \cdot K$
Q_{abs}	—	Absorbed energy, W
Q_c	_	Convective heat loss, W
Q_L	_	Loss energy, W
Q_r	_	Radiation heat loss, W
s	—	Specific entropy, kJ/kg
T_o	—	Environment temperature, K
w	—	Mass fraction
X	—	Salt fraction

Greek

α	—	Absorptivity of receiver
ξ	—	Optical efficiency of collector
τ	—	Transmission efficiency of receiver
σ	—	Stefan–Boltzmann constant
μ	—	Chemical potential

Subscripts

b	—	Brine
ch	—	Chemical
cs	—	Condensate
f	—	Feed
ke	—	Kinetic
o	—	Final state
pe	—	Potential
ph	—	Physical
s	—	Initial state
vs	—	Saturated vapour

Acknowledgements

The authors would like to thank Higher Education Commission (HEC), Govt. of Pakistan for the financial support in the form of NRPU # 5550 and Ghulam Ishaq Khan Institute of Engineering Sciences and Technology for providing support during the preparation of this work.

Data availability statement

The data that support the results of this manuscript are available on request to corresponding author.

References

[1] I.C. Karagiannis, P.G. Soldatos, Water desalination cost literature: review and assessment, Desalination, 223 (2008) 1–3.
[2] A.D. Khawaji, I.K. Kutubkhanah, J.M. Wie, Advances in seawater desalination technologies, Desalination, 221 (2008) 47–69.
[3] A.C. Duxbury, H. Robert, F.T. Mackenzie, Seawater Encyclopedia Britannica, Chicago, USA, 2021.
[4] UNICEF, Water Scarcity, Addressing the Growing Lack of Available Water to Meet Children's Need, UNICEF, New York, USA, 2021. Available at: https://www.unicef.org/wash/water-scarcity
[5] A. Boretti, L. Rosa, Reassessing the projections of the World Water Development Report, npj Clean Water, 2 (2019) 1–6.
[6] L. Raber, ACS honors Norbert Rillieux, evaporator, Chem. Eng. News, 19 (2002) 47–47.
[7] International Atomic Agency, Nuclear Desalination of Seawater, Proc. of a Symp. Taejon Republic of Korea, International Atomic Energy Agency (IAEA), Vienna, Austria, 1997, pp. 1–576.
[8] A. Ophir, F. Lokiec, Review of MED Fundamentals and Costing, Proc. of the Int. Conf. on Desalination Costings, IDE Technologies, Kadima, Israel, 2004, pp. 69–78.
[9] R. Semiat, Multi-Effect Distillation (MED), Water and Wastewater Treatment Technologies, Enc. of Life Supp. Sys., Springer Nature, Singapore, 2014.
[10] F.N. Alasfour, M.A. Darwish, A.O. Bin Amer, Thermal analysis of ME-TVC+MEE desalination systems, Desalination, 174 (2005) 39–61
[11] M.A. Darwish, Desalination Engineering, Balaban Desalination Publications, USA, 2015.
[12] P. Fiorini, E. Sciubba, Modular simulation and thermoeconomic analysis of a multi-effect distillation desalination plant, Energy, 32 (2007) 459–466.
[13] J. Belghaieb, W. Aboussaoud, M. Abdo, N. Hajji, Simulation and Optimization of a Triple-Effect Distillation Unit, 14th Conf. on Process Integration, Modelling and Optimisation for Energy Saving and Pollution Reduction, Florence, Italy, 2011, pp. 8–11.
[14] L. Roca, L.J. Yebra, M. Berenguel, A.D.L. Calle, Dynamic Modeling and Simulation of a Multi-Effect Distillation Plant, Proc. of the 9th Int. MODELICA Conf., Munich, Germany, 2012, pp. 883–888.
[15] Z.Q. Ma, S.H. Huo, M. Su, Simulation with ASPEN PLUS and performance analysis of LT-MED seawater desalination system, Appl. Mech. Mater., 397 (2013) 948–956.
[16] M.A. Sharaf, A.S. Nafey, L. García-Rodríguez, Exergy and thermo-economic analyses of a combined solar organic cycle with multi-effect distillation (MED) desalination process, Desalination, 272 (2011) 135–147.
[17] M.T. Ali, H.E.S. Fath, P.R. Armstrong, A comprehensive techno-economical review of indirect solar desalination, Renewable Sustainable Energy Rev., 15 (2011) 4187–4199.
[18] C. Ghenai, D. Kabakebji, I. Douba, A. Yassin, Performance analysis and optimization of hybrid multi-effect distillation adsorption desalination system powered with solar thermal energy for high salinity seawater, Energy, 215 (2021) 119212, doi: 10.1016/j.energy.2020.119212.
[19] M.W. Shahzad, K.C. Ng, K. Thu, B.B. Saha, W.G. Chun, Multi-effect desalination and adsorption desalination (MEDAD): a hybrid desalination method, Appl. Therm. Eng., 72 (2014) 289–297.
[20] A. Almutairi, P. Pilidis, N. Al-Mutawa, M. Al-Weshahi, Energetic and exergetic analysis of cogeneration power combined cycle and ME-TVC-MED water desalination plant: Part-1 operation and performance, Appl. Therm. Eng., 103 (2016) 77–91.
[21] C. Luo, N. Zhang, N. Lior, H. Lin, Proposal and analysis of a dual-purpose system integrating a chemically recuperated gas turbine cycle with thermal seawater desalination, Energy, 36 (2011) 3791–3803.
[22] Q. Chen, M. Burhan, M. Akhtar, F.H. Ybyraiymkul, D. Shahzad, M.W. Li, K.C. Ng, A decentralized water/electricity cogeneration system integrating concentrated photovoltaic/thermal collectors and vacuum multi-effect membrane distillation, Energy, 230 (2021) 120852, doi: 10.1016/j.energy.2021.120852.
[23] M.H. Sharqawy, J.H. Lienhard V, S.M. Zubair, Thermophysical properties of seawater: a review of existing correlations and data, Desal. Water Treat., 16 (2010) 354–380.

[24] M.H. Sharqawy, J.H. Lienhard V, S.M. Zubair, On exergy calculations of seawater with applications in desalination systems, Int. J. Therm. Sci., 50 (2011) 187–196.
[25] A. Almutairi, P. Pilidis, N. Al-Mutawa, M. Al-Weshahi, Exergetic and sustainability analysis of an intercooled gas turbine cogeneration plant with reverse osmosis desalination system, J. Energy Eng., 143 (2017) 04017016, doi: 10.1061/(ASCE) EY.1943-7897.0000445.
[26] T.T. Chow, Performance analysis of photovoltaic-thermal collector by explicit dynamic model, Sol. Energy, 75 (2003) 143–152.
[27] P. Palenzuela, D.C. Alarcón-Padilla, G. Zaragoza, Large-scale solar desalination by combination with CSP: techno-economic analysis of different options for the Mediterranean Sea and the Arabian Gulf, Desalination, 366 (2015) 130–138.
[28] J. Watmuff, D. Proctor, Solar and Wind Induced External Coefficients – Solar Collectors, Cooperation Mediterraneenne pour l'Energie Solaire, Revue Internationale d'Heliotechnique, World Organization of Mediterranean Cooperation for Solar Energy, France, 2nd Quarter, 1977, p. 56.
[29] B. Rahimi, A. Christ, K. Regenauer-Lieb, H.T. Chua, A novel process for low grade heat driven desalination, Desalination, 351 (2014) 202–212.
[30] GlobalPetrolPrices.com, Pakistan Electricity Prices, Neven Valev, USA, 2021. Available at: https://www.globalpetrolprices.com/Pakistan/electricity_prices/
[31] Forex, Currency Rates as per Pakistan Open Market, Forex, Pakistan, 2021. Available at: https://www.forex.pk/open_market_rates.asp
[32] Economic Research Institute, Sanitary Engineer Salary in Pakistan, ERI Economic Research Institute, Irvine, Canada, 2021. Available at: https://www.erieri.com/salary/job/sanitary-engineer/pakistan
[33] B. Rahimi, J. May, K. Regenauer-Lieb, H.T. Chua, Thermo-economic analysis of two novel low grade sensible heat driven desalination processes, Desalination, 365 (2015) 316–328.
[34] H.T. El-Dessouky, H.M. Ettouney, Fundamentals of Salt Water Desalination, Elsevier, USA, 2002.
[35] A.S. Nafey, H.E.S. Fath, A.A. Mabrouk, Thermo-economic investigation of multi effect evaporation (MEE) and hybrid multi effect evaporation-multi stage flash (MEE-MSF) systems, Desalination, 201 (2006) 241–254.
[36] A.S. Nafey, H.E.S. Fath, A.A. Mabrouk, Exergy and thermoeconomic evaluation of MSF process using a new visual package, Desalination, 201 (2006) 224–240.
[37] O.J. Morin, Cost aspects-MSF, Therm. Des. Proc., 2 (2010) 1–9.
[38] WASA, Revised Tariff for Commercial, Industrial, Non-Residential and Bulk Sewer Users, Lahore Development Authority, Water and Sanitation Agency (WASA), Lahore, Pakistan, 2021. Available at: https://wasa.punjab.gov.pk/system/files/tarrif-2017.pdf
[39] E.J.O. Promes, T. Woudstra, L. Schoenmakers, V. Oldenbroek, A. Thallam Thattai, P.V. Aravind, Thermodynamic evaluation and experimental validation of 253 MW integrated coal gasification combined cycle power plant in Buggenum, Netherlands, Appl. Energy, 155 (2013) 181–194.
[40] A. Olivieri, S. Ravelli, Cogasification of coal and biomass in an integrated gasification combined cycle power plant: effects on thermodynamic performance and gas composition, J. Energy Eng., 146 (2020) 04020071, doi: 10.1061/(ASCE) EY.1943-7897.0000716.
[41] B. Maha, S. Ali, B.B. Ammar, Modeling and Simulation of Multi-Effect Desalination Plant (SIDEM Unit), 2017 International Conference on Green Energy Conversion Systems (GECS), IEEE, Hammamet, Tunisia, 2017, pp. 1–6.
[42] M.J. Rahimi, M.H. Hamedi, M. Amidpour, Thermodynamic and economic evaluation of a novel configuration for sustainable production of power and fresh water based on biomass gasification, Energy Syst., 12 (2019) 61–106.
[43] K.M. Chehayeb, J.H. Lienhard V, Effect of Feed Salinity on the Performance of Humidification Dehumidification Desalination, The International Desalination Association World Congress on Desalination and Water Reuse 2015/San Diego, CA, USA, 2015, pp. 1–17.
[44] J. Xue, Q. Cui, J. Ming, Y. Bai, L. Li, Analysis of thermal properties on backward feed multi-effect distillation dealing with high-salinity wastewater, J. Nanotechnol., 2015 (2015) 1–7.